Dyes and Pigments 240 (2025) 112867

Contents lists available at ScienceDirect

Dyes and Pigments

journal homepage: www.elsevier.com/locate/dyepig

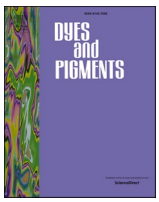

Copolyformals containing metalloporphyrins as solid optical probes for amines detection

Lidia Mezzina [a], Angelo Nicosia [a,*], Placido G. Mineo [a,b]

[a] Department of Chemical Sciences and INSTM UdR of Catania, University of Catania, V.le A. Doria 6, Catania, I-95125, Italy
[b] Institute for Chemical and Physical Processes, National Research Council (IPCF-CNR), Viale F. Stagno d'Alcontres 37, I-98158, Messina, Italy

ARTICLE INFO

Keywords:
Porphyrin
Polyetherformal
Optical sensing
Volatile organic compounds
Amine
Polymeric sensor

ABSTRACT

A polymer-based sensor incorporating porphyrin species as the sensing unit, which makes it able to detect different volatile organic compounds (VOCs) of environmental and industrial relevance, was developed by synthesizing copolyetherformals with metalloporphyrin units in the main chain. Particularly, the Zinc and Cobalt -porphyrins were produced by metalation of the porphyrin moiety into the copolyetherformal. The structural and chemical-physical features of the obtained systems were investigated by means of MALDI-TOF mass spectrometry, gel permeation chromatography, UV–Vis, fluorescence and nuclear magnetic resonance spectroscopies, as well as thermoanalyses techniques. The sensing properties of the copolymers were evaluated in toluene solutions and in solid-state thin film. In solution, the zinc-porphyrin-containing copolymer exhibited a linear response in the range of 60 μM to 0.7 mM for pyridine and approximately 1.1 μM–60 μM for piperidine. The cobalt-porphyrin-containing copolymer exhibited a linear response in the range of approximately 0.3 μM–30 μM for pyridine and about 0.09 μM–18 μM for piperidine. The performance of the sensors was further investigated in the solid state by exposing the thin films of the copolymer sensors to VOCs, showing sensing features towards the amine species and no sensing activity towards the ethers and aromatic nonpolar species. These findings underline the potential of metalloporphyrin-polymeric systems as versatile and highly sensitive materials for VOCs optical sensing applications.

1. Introduction

The detection of Volatile Organic Compounds (VOCs) is of critical importance in environmental monitoring and industrial applications due to their ubiquitous presence and potential health hazards [1,2]. Among VOCs, amines are extensively emitted from anthropogenic activities such as animal husbandry and biomass combustion [3,4], as well as the food industry [5,6]. Their emission into the troposphere facilitates interactions with water and particulate matter, which supports their global diffusion through multiple pathways [7]. Considering their widespread presence and potential environmental impacts [8,9], the development of efficient and selective sensing systems for amines is imperative. Furthermore, biogenic amines typically originate in foods through the decarboxylation of amino-acids, resulting in a variety of hazardous substances [10] that could affect human health, thereby underscoring the importance of their rapid detection [11–13].

Porphyrins and metalloporphyrins constitute a class of macromolecules that have garnered significant attention in various scientific fields [14–16], particularly in the development of sensing applications [17–21]. These compounds are recognized for their remarkable optical and electronic properties, which exhibit high sensitivity to interactions with various chemical species [21–23]. Their versatility stems from their ability to coordinate metals within the porphyrinic core, thereby altering their chemical, electronic, and optical properties. Metalloporphyrins, thanks to their ability to interact with electron-donor molecules, thereby inducing substantial alterations in their absorption and/or emission spectrum, acts as molecular sensors proficient in detecting a broad spectrum of analytes across environmental, industrial, and biological contexts [17,24–27].

Among the various metal ions that can be incorporated into the porphyrinic core, Cobalt and Zinc are two of the most studied. Cobalt-porphyrin complexes are renowned for their pronounced affinity for nitrogen-containing ligands, which facilitates their function as effective sensors for amines and related compounds [28]. Conversely, Zinc-porphyrin complexes are notable for their optical features, although they tend to be less efficient in coordination chemistry than

* Corresponding author.
E-mail address: angelo.nicosia@unict.it (A. Nicosia).

https://doi.org/10.1016/j.dyepig.2025.112867
Received 23 February 2025; Received in revised form 29 April 2025; Accepted 30 April 2025
Available online 1 May 2025

their Cobalt-based counterparts [29,30].

An important consideration in the development of functional sensors using porphyrins is the requirement for materials that exhibit both stability and processability. Porphyrins present challenges in handling when used as standalone materials due to their propensity to aggregate [31,32], their limited solubility in numerous solvents [33], and their insufficient mechanical properties for the formation of stable thin films [34]. To address these challenges, an adaptable strategy may involve embedding of porphyrins in polymeric matrices [35,36].

Polymeric matrices offer several advantages in the development of thermoplastic filmable materials [37,38], as they function as carriers capable of homogeneously dispersing porphyrin molecules [39]. Nonetheless, when a physical mixture of a polymer with porphyrins is prepared, the porphyrins may migrate within the polymer matrix, resulting in phase segregation [40,41] which adversely affects the efficiency of the sensor. With the objective of developing robust and filmable sensors applicable in diverse liquid and gaseous sensing environments, a synthetic strategy specifically designed to guarantee the immobilization of porphyrins within the polymer matrix can be achieved through the functionalization of the porphyrin peripheral position with appropriate groups to allow its covalent bond within a polymer matrix [35,42,43]. A useful approach is based on condensation reaction leading to step-growth polymers, such as copolyetherformals, These are thermostable polymers having good chemical and physical properties, that were already used to produce polymeric optical sensors thanks to their transparency in the visible wavelength region [44–46].

Furthermore, polymeric systems can be easily applied to diverse surfaces using techniques such as spin-coating [47], dip-coating [48], or spraying [49]. This facilitates the integration of porphyrin-based sensors into devices suitable for applications that require sensors that are flexible, durable, and capable of covering large surface areas [47].

In this study, to address the challenges mentioned above, a copolyformal incorporating porphyrins within the main chain was synthesized using dibromomethane, bisphenol-A, and 5,15-(4-hydroxyphenyl)-5,20-(diphenyl)-21H,23H-porphine as comonomers. Polymerization was performed through an interfacial polycondensation reaction. The resultant copolyformal exhibited thermal stability and filmability. To enable the system to be sensitive to electron donor species, the porphyrin moiety within the copolymer underwent metalation reactions to yield the corresponding Cobalt- and Zinc-porphyrin complexes. The investigation of the structural, compositional and chemical-physical features was carried out using MALDI-TOF mass spectrometry, gel permeation chromatography (GPC), thermoanalytical techniques, as well as UV–Vis, fluorescence, and ^{1}H NMR spectroscopies.

Finally, sensing features of the copolymers were verified against polar and non-polar volatile compounds. Experimental data showed that the copolymers can detect pyridine and piperidine, and remain inactive towards THF and toluene.

The data obtained indicated the metalloporphyrin-polymeric systems as a potential versatile and highly sensitive materials suitable for a wide range of VOCs sensing applications.

2. Materials and methods

Tetrahydrofuran (THF), n-hexane, ethanol (EtOH), methanol (MeOH), water (LC-MS grade), dichlorometane (CH_2Cl_2), chloroform ($CHCl_3$), deuterated chloroform ($CDCl_3$), pyridine, triethylamine (TEA), sodium hydroxide, potassium hydroxide, dibromomethane, Tetrabutylammonium bromide (TBAB), piperidine and bisphenol-A (BPA) were purchased from Sigma Aldrich. 5,15-(4-hydroxyphenyl)-5,20-(diphenyl)-21H,23H-porphine (P) was obtained from Frontier Specialty Chemicals.

2.1. Polyetherformal synthesis

Polyetherformal (PEF), used as reference, was synthesized by interfacial polycondensation using TBAB as a phase transfer agent [50]. Briefly, sodium hydroxide (660.0 mg, 16.5 mmol), TBAB (236.0 mg, 0.733 mmol) and BPA (167.0 mg, 0.73 mmol) were solubilized in water (5 mL). Concurrently, dibromo-methane (51 μL, 0.73 mmol) was dispersed in toluene (5 mL). The two solutions were mixed and heated at 110 °C under vigorous stirring for 24 h. The organic phase was subsequently precipitated twice in acidulated methanol (40 mL of methanol with 1.6 mL of acetic acid). The solid sample collected was dried in a vacuum oven (80 °C, 24 h), resulting in a yield of approximately 39 %.

The copolymer, incorporating the porphyrin moiety within the main chain and designed as PEF-P, was synthesized utilizing an analogous methodology. In summary, sodium hydroxide (660.0 mg, 16.5 mmol), TBAB (240 mg, 0.745 mmol), BPA (150 mg, 0.660 mmol), and P (25 mg, 0.039 mmol) were dissolved in water (5 mL) using an ultrasonic bath treatment for 15 min at 50 °C. Separately, dibromo-methane (51 μL, 0.73 mmol) was dissolved in toluene (5 mL). The two solutions were combined and the reaction was carried out under continuous stirring for 24 h at 100 °C. Finally, PEF-P was isolated by precipitation in acidulated methanol (40 mL of methanol with 1.6 mL of acetic acid) and subjected to vacuum drying for 24 h at 80 °C, resulting in a yield of about 38 %.

2.2. Metalation of the copolyether PEF-P

The metalation reaction of PEF-P was performed as reported in the literature [51]. Briefly, PEF-P (approximately 15 mg) was dissolved in pyridine (3 mL) and metal acetate (Co(II) or Zn(II)) was added to the solution in appropriate amounts to obtain a porphyrin:metal molar ratio of 1:10. The mixture was stirred under a nitrogen atmosphere and kept at 100 °C for 24 h.

The residue, once dissolved in THF, was purified through a silica-gel chromatography column to remove any unreacted salt. The eluate was preliminarily dried with a nitrogen stream and then in a vacuum oven at 50 °C. To remove the residual coordinated pyridine, the copolymer was dissolved in toluene and washed twice with diluted hydrochloric acid using a separating funnel. The organic phase was then recovered and dried using a nitrogen stream followed by a vacuum oven treatment at 50 °C for 24 h, yielding 97.6 % and 82.0 % for the Cobalt (PEF-PCo) and Zinc (PEF-PZn) derivatives, respectively.

2.3. Sensing properties

The sensing properties of PEF-PCo and PEF-PZn were examined in solution and as a solid thin film.

For solution-based assessments, the copolymeric system was dissolved in toluene (1 mg/mL) and then diluted to reach a concentration of 0.1 mg/mL. For solid-state tests, the copolymer (either PEF-PCo or PEF-PZn) was deposited on a polyethylene terephthalate (PET) film (disks with diameter ~1 cm) by solvent casting (100 μL of PEF-PMe THF solution, 0.5 mg/mL), and allowed to dry overnight at 50 °C.

The resulting film was placed in the headspace of a glass vial (20 mL) containing 100 μL of the selected pollutant. The vial was sealed and positioned on a heating plate at 50 °C to ensure the saturation of the headspace with the vapors of the pollutant, preventing the occurrence of condensation phenomena. UV–visible diffuse reflectance spectroscopy (DRS) measurements were then performed on the polymeric film to evaluate its response following the exposure to the gaseous pollutant. The stability of the sensor was verified through three reuse cycles: after the exposure to the pollutant, the solid sensor was recovered through vacuum oven treatment (1 h, 50 °C).

2.4. Instruments

MALDI-TOF mass spectra were acquired in linear mode with a Voyager DE (PerSeptive Biosystem) and using the delay extraction device (25 kV after 2600 ns, potential gradient 454 V mm^{-1}, wire voltage 25 V) [52,53]. The calibration of the mass spectrometer was performed

as previously described [54]. The *trans*-2-[3-(4-*tert*-butylphenyl)-2-methyl-2-propenylidene] malononitrile (DCTB) was used as a matrix. The data analysis was performed with the Grams/386 software (Version 3.04, Galactic Industries Corp) [55]. The *m/z* value reported in the text are referred to the most abundant isotopes in the macromolecule.

^{1}H NMR spectra were registered at 27 °C with a ^{UNITY}INOVA instrument (Varian, Agilent Technologies) operating at 500 MHz. Spectra acquisition and processing were performed with the VnmrJ software (Version 2.2C, Varian, Agilent Technologies). The samples were dissolved in deuterated chloroform and the chemical shifts were expressed in ppm, using TMS signal as a reference.

Gel permeation chromatography (GPC) experiments were performed using a PL-GPC 110 (Polymer Laboratories), equipped with two Mixed-D and one Mixed-E PL-gel 5 μm columns joined in series. As detectors, a differential refractometer connected in parallel with a UV–Vis spectrophotometer (Hewlett Packard series 1050) were used. The analysis was performed at 35 ± 0.1 °C using THF as eluent (flow rate 1 mL min^{-1}). Data acquisition was performed with ASTRA software (version 6.0.1.10, Wyatt Technology) [56]. The average molecular mass values (Mw and Mn) were calculated using monodisperse polystyrene samples as standards (from Polymer Laboratories, mass range from 2.05 KDa to 1.2 MDa).

Thermogravimetric analyses (TGA) were performed in the temperature range 50–800 °C (thermal ramp of 10 °C min^{-1}) in nitrogen atmosphere (60 mL min^{-1}) using a TGA 7 equipped with a TAC 7/DX (PerkinElmer).

Differential scanning calorimetry (DSC) measurements were performed with a TA Q20 equipped with a refrigerant cooling system (RCS-90), applying a heating rate of 10 °C min^{-1}, in an anhydrous nitrogen atmosphere (60 mL min^{-1}).

UV–Vis spectra were acquired using a Cary60 UV–Vis spectrophotometer (Agilent Technologies), with quartz cuvettes (1 cm path length) and THF or toluene as solvent (T = 25.0 ± 0.1 °C). UV–Vis diffuse reflectance Spectroscopy (DRS) spectra were recorded using a V-670 spectrophotometer (Jasco Corporation) equipped with an ISV-722 integrating sphere (Jasco Corporation). Fluorescence spectra were obtained with an FP-8200 spectrofluorometer (Jasco Corporation), in quartz cuvettes (1 cm path length) and using THF or toluene as solvent.

The UV–Vis and fluorescence spectra were analyzed using the Spectragryph optical spectroscopy software (version 1.2.11, Dr. F. Menges) [57].

3. Results and discussion

The development of a polymer containing porphyrinoid species used as the sensing element was carried out by introducing 5,15-(4-hydroxyphenyl)-5,20-(diphenyl)-21H,23H-porphine (P) as a repeating unit of a copolyetherformal, named PEF-P. To optimize the optical density of the system, the concentration of P in PEF-P was maintained at approximately 5 %mol. The polymerization was conducted through a water/toluene interfacial reaction, using TBAB as a phase transfer agent. Specifically, P, BPA, and TBAB were solubilized in water (adjusted to pH 12, approximately). The dibromo-methane was added to the toluene phase. The biphasic toluene-water mixture produced was subjected to 24 h of vigorous stirring at 100 °C in a nitrogen atmosphere (Fig. 1a). Owing to the nature of the polymerization method and the similar reactivity of the comonomers, it is reasonable to assume the formation of a statistical copolymer. As a blank system, a polyether formal containing only BPA (named PEF) was synthesized in the same way and used to assess the effect of the porphyrin moiety on the polymer matrix (Fig. 1b).

The structure of the polymers was investigated by MALDI-TOF mass spectrometry. The mass spectrum of PEF (Fig. S1a) shows clusters of peaks at *m/z* 1223.3 + *n*240 (°) and 1479.5 + *n*240 (*) (*n* = 0–17, starting from pentameric cyclic species) attributed to the cyclo-[[BPA-CH_2]$_n$] Na^+ and K^+ species, respectively. The mass spectrum of PEF-P (Fig. S1b) shows main peaks at *m/z* 1139.1 +*n*240 (#) (*n* = 0–17) due to the cyclo-[[BPA-CH_2]$_n$-[P–CH_2]$_1$] H^+ species, at *m/z* 1223.3 + *n*240 (°) (*n* = 0–17) due the cyclo-[[BPA-CH_2]$_n$] Na^+ species.

The molecular structure of the polymers was confirmed by ^{1}H NMR spectroscopy. In particular, the spectrum of PEF shows the following signals (Fig. S2): two doublets at 7.10 ppm and 6.98 ppm (both 4H, C–H aryl, **a** and **b**, respectively), a singlet at 5.63 ppm (2H, C–H methylene, **d**), a singlet at 1.60 ppm (6H, C–H methyl, **c**). The ^{1}H NMR spectrum of the PEF-P (Fig. 2) shows, in addition to the signals of PEF, also the signals of the porphyrinic comonomer (protons amount is relative to the porphyrin structure): a multiplet at 8.82 ppm (8H, C–H pyrrole protons in **e** positions); two unresolved multiplets from 8.22 to 8.09 ppm (8H,

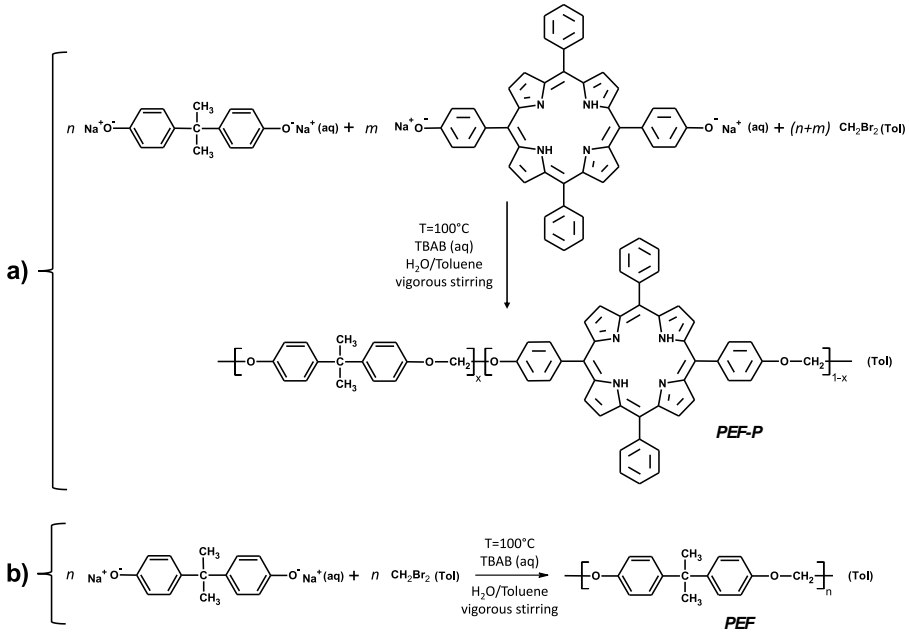

Fig. 1. Scheme of the PEF-P (a) and PEF (b) polyether formals syntheses.

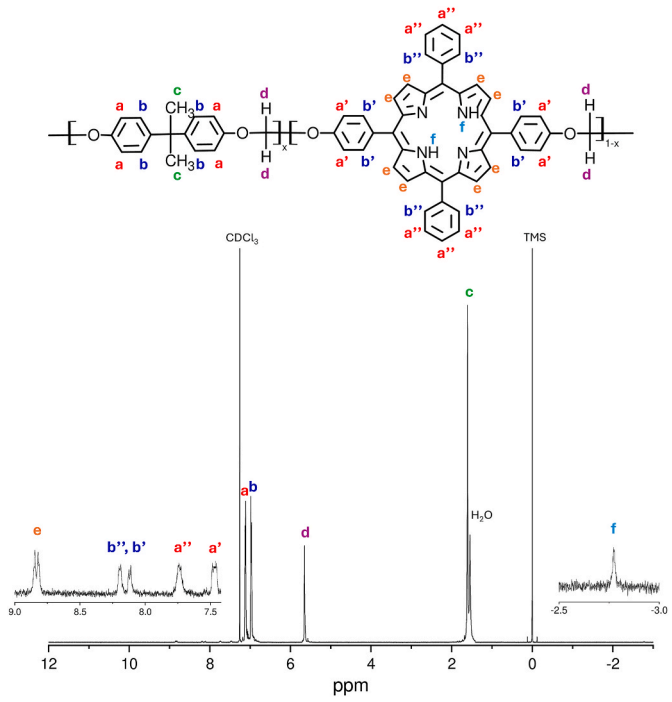

Fig. 2. ^{1}H NMR spectrum of PEF-P.

C–H phenyl protons, **b''** and **b'**); a multiplet at 7.71 ppm (6H, C–H phenyl protons, **a''**); a multiplet at 7.43 ppm (4H, C–H phenyl protons, **a'**); a singlet at −2.78 ppm (2H, N–H pyrrole protons, **f**).

The GPC analysis of PEF (Fig. S3) shows a broad band at the RI detector, without any absorbance at the UV–Vis detector set at 420 nm. The average molecular weights of the PEF result to be Mn = 6.7 kDa and Mw = 17.1 kDa (PDI = 2.55). On the other hand, the GPC analysis of PEF-P (Fig. 3) confirmed the homogeneous presence of P moieties within the main chains of the copolymer, as evidenced by the overlap of the refractive index and UV–Vis (set at 420 nm, which is the absorbance wavelength of the porphyrinic moiety) detectors traces. The average molecular weights of the copolymer result to be Mn = 4.0 kDa and Mw = 21.1 kDa (PDI = 5.20). The observed multimodal molecular mass distribution is attributed to the formation of both linear and cyclic species [45,58–61].

Thermogravimetric analysis was performed under a nitrogen atmosphere to verify the thermal behavior of the polymers. For PEF (Fig. 4, black line), an initial weight loss step of 2 % was observed at 95 °C, which is attributed to the loss of solvent residues. The main weight loss occurs at 418 °C (PDT 450 °C), which is attributed to the thermal degradation of the polymer, resulting in a residue at 800 °C of 12 %. Regarding the thermal degradation pathway, polyether formals undergoes thermal degradation through the formation of cyclic oligomers comprising two or three repeating units, along with thermal rearrangement that produces compounds with aldehyde, hydroxyl, methyl, and phenyl end groups [62,63].

Conversely, the TGA trace for PEF-P (Fig. 4, red line) exhibits slightly reduced thermal stability relative to homopolymer (T_{onset} = 398 °C, PDT = 439 °C), with a higher residual amount at 800 °C (26 %), owing to the contribution of the porphyrin's extended aromatic structure [50].

On the other hand, incorporation of porphyrin within the main chain of the polymer exerts minimal impact on the glass transition temperature (Tg) of the system, which is recorded at 89.08 °C for PEF and 90.06 °C for PEF-P (Fig. 4 inset).

Although P is integrated into the polymeric chain, its spectroscopic properties are almost retained. The THF solutions of P and PEF-P exhibit the characteristic porphyrin-like absorption spectra (Fig. 5 red and blue solid lines, respectively), showing the Soret band at λ = 418 and 417 nm (originating from the S_0–S_2 electronic transition [64,65]), respectively, and four Q-bands at 515 nm, 550 nm, 594 nm, and 650 nm (due to the S_0–S_1 electronic transitions [32]). Considering the molar absorption coefficient of P (226000 $M^{-1}cm^{-1}$), the percentage amount of P within the PEF-P was determined to be approximately 1.9 %mol (5.5 %w) with respect to BPA.

Regarding the fluorescence properties of both P and PEF-P, upon excitation of the solution at a wavelength of 430 nm, the emission spectrum exhibited the maximum at 653 and 651 nm (Fig. 5, red and blue dashed lines), respectively.

Consistent with observations in porphyrinoids [66–69], the PEF-P system also showed solvatochromism phenomenon. The UV–Vis spectra of PEF-P, acquired in toluene solution (Fig. 6, continuous black line), exhibited the Soret band at 420 nm, and four Q-bands at 515.5, 551, 596, and 652 nm. As expected, metalation of the P core within the copolyformal structure modifies the spectroscopic properties due to changes in the electronic structure and symmetry of the porphyrin macrocycle [65]. The PEF-PZn absorption spectrum (Fig. 6, continuous red line) exhibited a sharp Soret band at 424 nm and two Q-bands at 551 and 592 nm. On the other hand, the PEF-PCo UV–Vis spectrum exhibited

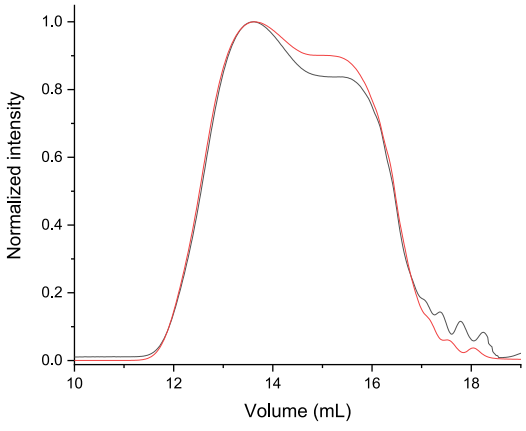

Fig. 3. GPC traces of PEF-P using refractive index (black line) and UV–Vis (set at 420 nm, red line) detectors connected in parallel. (For interpretation of the references to colour in this figure legend, the reader is referred to the Web version of this article.)

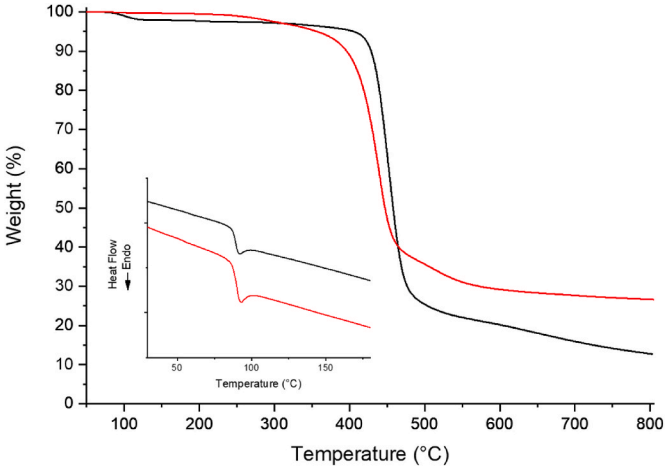

Fig. 4. TGA and DSC (inset) analyses of PEF (black lines) and PEF-P (red lines). (For interpretation of the references to colour in this figure legend, the reader is referred to the Web version of this article.)

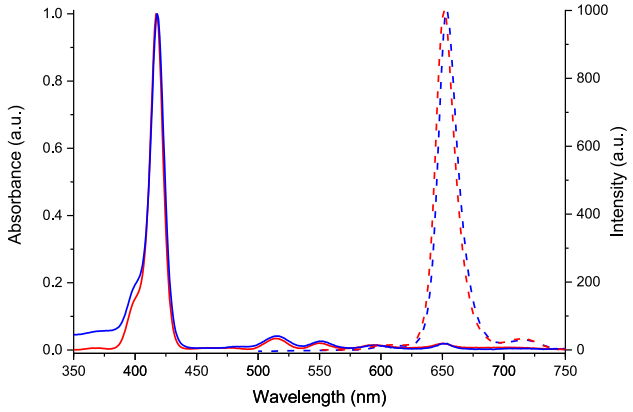

Fig. 5. Absorption (continuous line) and emission spectra (dashed line, λ_{exc} = 430 nm) of PEF-P (red lines) and P (blue lines) in THF solution. (For interpretation of the references to colour in this figure legend, the reader is referred to the Web version of this article.)

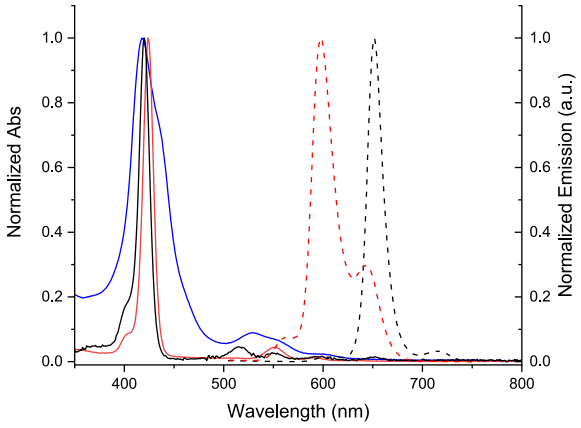

Fig. 6. Normalized absorption (solid line) and normalized emission spectra (dashed line) of PEF-P (black lines, λ_{exc} = 430 nm), PEF-PZn (red lines, λ_{exc} = 430 nm) and PEF-PCo (blue line) in toluene solution. (For interpretation of the references to colour in this figure legend, the reader is referred to the Web version of this article.)

(Fig. 6, continuous blue line) a broad Soret band with a maximum at 418 and a shoulder at 434 nm. This broadening of the band may result from partial aggregation of the PCo moiety within the PEF-PCo structure, possibly due to the interaction between the metal center and the aromatic core of adjacent porphyrins. Additionally, broad Q-bands appear at 529 nm, with a shoulder at 555 nm, and at 602 nm.

Regarding fluorescence emission, PEF-PZn (Fig. 6, dashed red line) showed a main emission band at 598 nm (λ_{exc} = 425 nm) overlapped with a secondary band at 644 nm. Comparison with the PEF-P fluorescence emission (Fig. 6, dashed black line) reveals that the inclusion of the Zn cation induces a blue shift in the fluorescence emission. Conversely, the inclusion of the Co cation within the P core induces quenching of the fluorescence emission (data not shown for brevity).

3.1. Sensing toward amines species

Metallo-porphyrins are renowned for their spectroscopic properties, which makes them suitable for the detection of electron-donor species, such as amines. This occurs by coordination between the nitrogen atoms in these species and the central metal cation within the porphyrin core, leading to modifications in its spectroscopic features. Same kind of coordination with oxygen-based electron-donor species (as an example, THF) is not occurring in our systems, as confirmed by experiments with PEF-PZn and PEF-PCo in toluene solution (data not shown for brevity).

On the other hand, after exposure to amino derivative species [70], the toluene solution of PEF-PZn exhibited substantial changes in both absorbance and emission spectra (Fig. 7). Specifically, the addition of pyridine to the PEF-PZn solution (Fig. 7a) results in a bathochromic shift in both the Soret band, shifting from 424 nm to 429 nm, and the Q-bands, comprising a 12 nm shift from 551 nm to 563 nm, along with a decrease in intensity, and an 11 nm shift from 593 nm to 604 nm, accompanied by an increase in intensity.

The observed spectral variations are slightly more pronounced in the presence of non-aromatic amino species, such as piperidine (Fig. 7c), exhibiting a bathochromic shift of the Soret band of 7 nm (from 424 nm to 431 nm) as well as the Q-bands, shifting from 14 nm from 551 nm to 565 nm, accompanied by a decrease in intensity, and a shift of 12 nm (from 593 nm to 605 nm) with an increase in intensity.

This difference likely arises from the nature of piperidine nitrogen, which possesses a more available lone pair, making it a more proficient electron donor species toward Zinc cation in the PEF-PZn. In contrast, in aromatic systems such as pyridine, the nitrogen's lone pair tends to be less available due to electron delocalization within the aromatic ring, thus reducing the ability of nitrogen to interact with other species [71], as already reported for other Zn(II) porphyrinoids [69].

Regarding the coordination chemistry, the Zinc cation within the porphyrin core, typically, exhibits a preference for tetrahedral or square-pyramidal geometries, depending on the ligands involved [72,73], exhibiting a five-coordination behavior in solution [69]. In terms of the electronic perturbation, when nitrogen coordinates the Zinc-porphyrin, it alters the energy levels of the molecular orbitals of the metal-porphyrin system, affecting the transition energies determining the modification of absorbance and emission phenomena [74,75].

Examining the emission spectrum, in presence of pyridine and piperidine (Fig. 7b and d), a similar behavior is observable for both. Specifically, it is evident a decrease in the intensity of the band at 597 nm, accompanied by a shift to 610 nm, as well as a lowering of the band at 644 nm with a shift to 660 nm. Considering the UV–Vis spectra, the PEF-PZn system exhibited a linear response within the range of 60 μM to 0.7 mM for pyridine (LOD = 22 μM), and approximately 1.1 μM–60 μM for piperidine (LOD = 0.5 μM). As expected, the fluorescence emission ensures a wider range of linear response for both the pollutants, going from 80 μM to 3 mM for pyridine (LOD = 38 μM) and from 3.6 μM to 0.1 mM for piperidine (LOD = 1.2 μM).

The sensing properties of the PEF-PZn system were further investigated by employing PEF-P in the form of a solid thin film, through its exposure to vapors of pollutants and subsequent monitoring of the optical response via DRS. The presence of gaseous toluene or THF do not induce any spectroscopic change (data not shown). In the presence of pyridine, after 1 min of exposure, the diffuse reflectance spectrum of PEF-PZn thin film (Fig. 8a) exhibited a quick shift in the Soret band, from 427 to 433 nm. The interaction with piperidine (Fig. 8b) induces analogous spectral changes, characterized by a shift in the Soret band from 427 to 434 nm. However, for piperidine, the intensity variation is slightly more pronounced, and the formation of a new side band at 465 nm is evident. This phenomenon corroborates the trends observed in liquid-phase experiments, wherein the formation of the complex with PEF-PZn is significantly affected by the structure of the amino derivative pollutant, whether aromatic or non-aromatic. The reusability of the solid sensor was verified up to three cycles, with a performance decrease below 5 % (inset Fig. 8a and b).

The sensing feature of PEF-PCo was investigated by monitoring changes in its absorption spectrum upon exposure to amine species, varying the concentrations of pyridine and piperidine (Fig. 9a and b).

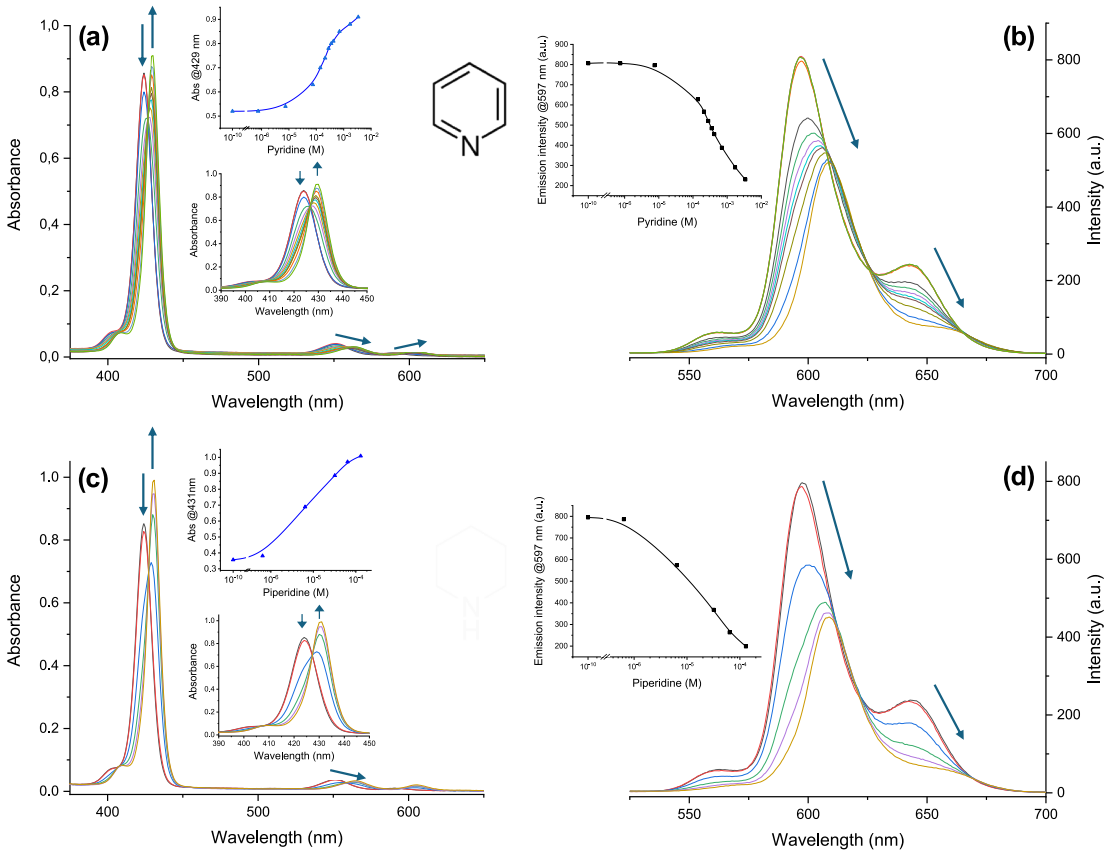

Fig. 7. Absorption (a, c) and emission (b, d) spectra of PEF-PZn in toluene solution (0.1 mg/mL) with increasing concentrations of pyridine (a and b) and piperidine (c and d). In the inset, the variation of the absorbance or fluorescence emission at 429 nm (a), 597 nm (b), 431 nm (c) and 597 nm (d). The enlarged representation (wavelength range 390–450 nm) of the spectra, showing the isosbestic point within the absorption titration spectra, is reported in the insets of (a) and (c).

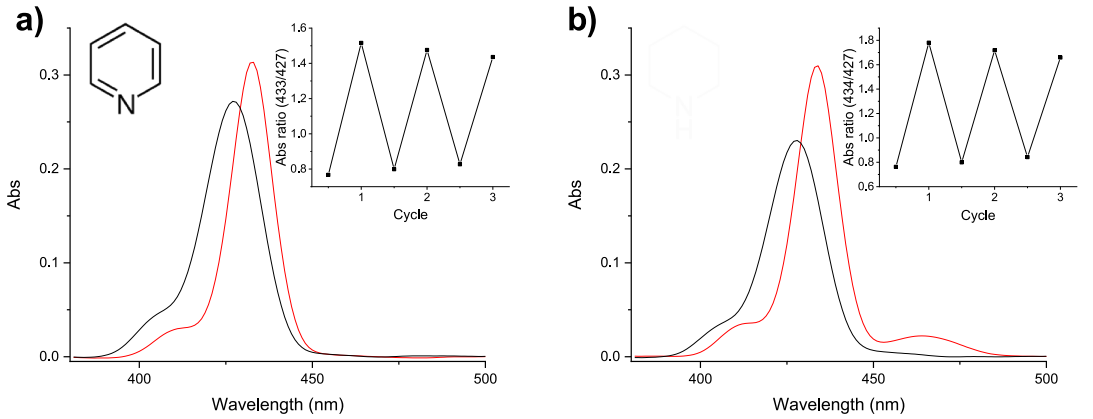

Fig. 8. Diffuse reflectance spectra of PEF-PZn thin film deposited onto PET (black lines) and exposed to Pyridine (a) and Piperidine (b) (red lines). Inset shows the variation of the absorbance intensity ratio registered during three reuse cycles. (For interpretation of the references to colour in this figure legend, the reader is referred to the Web version of this article.)

The experiment in toluene solution was performed by increasing the concentration of pyridine, revealing a notable red-shifts in the Soret band, about 20 nm from 417 nm to 438 nm, and in the Q-bands, from 528 to 697 nm to 556 and 603 nm, respectively (Fig. 9). This phenomenon is attributed to the coordination of pyridine's nitrogen with PEF-PCo [76].

In the presence of piperidine, the absorption spectrum of the solution of the PEF-PCo complex exhibited similar spectral changes, even if starting at lower concentrations of pollutant, as expected due to the more readily available electron lone pair of piperidine.

The enhanced sensitivity of Co-porphyrin compared to Zn-porphyrin is primarily ascribed to differences in their electronic structure and

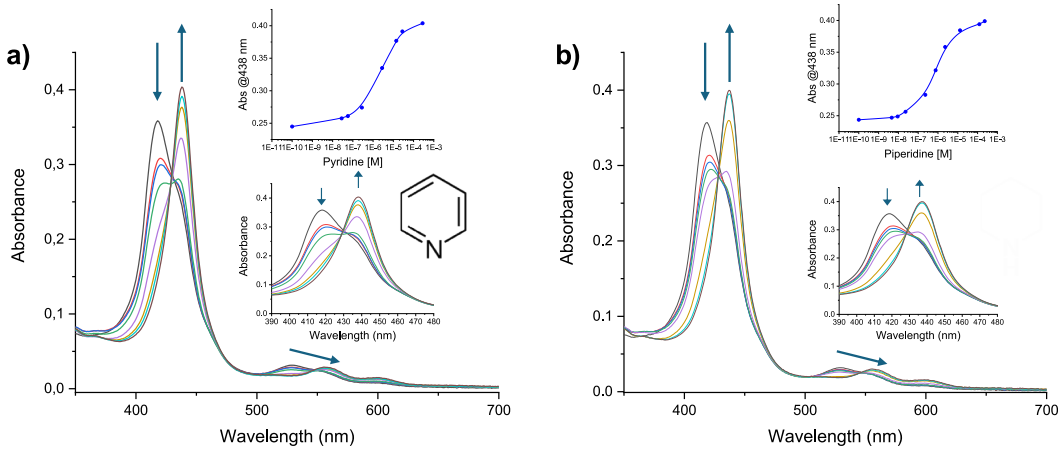

Fig. 9. Absorption spectra of PEF-PCo in toluene solution (0.1 mg/mL) with increasing concentration of pyridine (a) and piperidine (b). In insets, the variation of the intensity of the new Soret band at 438 nm (blue line) and the enlarged representation in the wavelength range 390–480 nm. (For interpretation of the references to colour in this figure legend, the reader is referred to the Web version of this article.)

coordination chemistry. Specifically, PEF-PCo demonstrated a linear response ranging from approximately 0.3 μM–30 μM for pyridine (LOD = 0.16 μM) and from about 0.09 μM to 18 μM for piperidine (LOD = 0.04 μM). The Co(II) is recognized to have a flexible and reactive coordination environment, which generally makes it prone to binding to nitrogen ligands [77,78].

In particular, the partially filled d-orbitals of Co(II) facilitate stronger metal-ligand interactions compared to those of Zn(II), which possesses a completely filled d-shell. This results in a more stable coordination bond in Co-porphyrin complexes, which accounts for the increased sensitivity to both pyridine and piperidine [74] with respect to PEF-PZn. Concerning the emission spectra of PEF-PCo, the quenching effect exerted by the Cobalt cation avoids the observation of any significant emission signal.

DRS UV–Vis spectrum of the thin films of PEF-PCo exhibited (Fig. 10) a broad absorption band centered approximately at 434 nm. The broadening of the PEF-PCo Soret band may be attributed to the interaction between the Cobalt and the pyrrole ring of adjacent porphyrins [79]. The exposure to gaseous toluene or THF not determines significant alteration of the UV–vis spectrum. Conversely, exposure to pyridine and piperidine vapors over 1 min results in an evident spectroscopic variation. In particular, the interaction with pyridine (Fig. 10a) leads to the formation of a sharp band at 440 nm. Instead, the interaction with piperidine (Fig. 10b) results in a slightly more intense band centered at 437 nm with a shoulder at 417 nm. The performances of the solid sensor were retained up to three reuse cycles (inset in Fig. 10a and b).

To verify the effectiveness of the metals within the porphyrin core, similar sensing experiments were performed using PEF-P as sensor. As expected, no spectral variations were observed (data not reported for brevity). On the other hand, using other polar and non-polar organic substances, such as THF and toluene, no spectra variations were observed.

In order to correlate the experimental findings acquired in solution with the chemical nature of the host-guest systems, a preliminary evaluation of the association constants (K_a) was performed by applying Eq. (1).

$$K_a = \frac{[PEF - PMe + Pollutant]}{[PEF - PMe][Pollutant]} \quad \text{Eq. 1}$$

In this equation, the term *[PEF-PMe + Pollutant]* represents the concentration of the PEF-PCo/pollutant complex at the inflection point of the titration, whereas as *[PEF-PMe]* and *[Pollutant]* indicate the concentrations of metalloporphyrin and the pollutant. The results obtained are reported in Table 1, where the differences in the binding capabilities

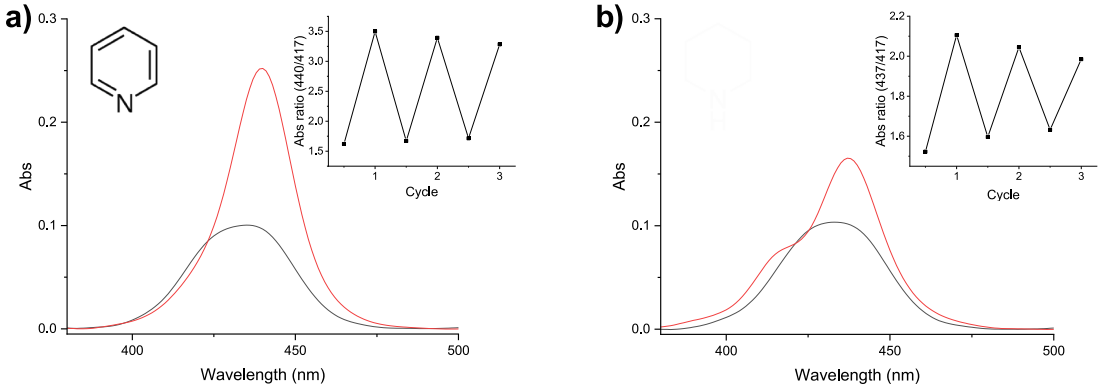

Fig. 10. Diffuse Reflectance UV–Vis spectra of PEF-PCo thin film deposited onto an acetate substrate in the presence of Pyridine (a) and Piperidine (b), before (black line) and after (red line) exposure. Inset shows the variation of the absorbance intensity ratio registered during three reuse cycles. (For interpretation of the references to colour in this figure legend, the reader is referred to the Web version of this article.)

Table 1
Association constants (log K) of the sensor systems towards different pollutants. The pK_a values are reported from Ref. [69].

Polymer Sensor	Pyridine pK_a = 5.23	Piperidine pK_a = 11.22
PEF-PZn	3.7	4.9
PEF-PCo	5.3	5.9

due to the metal placed at the center of the porphyrinic core and the electron-donor ability of the different pollutant result to be evident [80, 81].

4. Conclusions

Copolyformals incorporating porphyrin derivatives in the main chain were synthesized through an interfacial TBAB assisted polycondensation reaction. The synthetic route resulted in a high average molecular weight copolymer (Mw = 21.1 kDa, PDI = 5.20) possessing a film-forming abilities. MALDI-TOF mass analysis identified the presence of linear and cyclic species containing porphyrinic units. The spectroscopic properties of P were preserved even when it was incorporated in the PEF-P structure, exhibiting only minimal shifts of a few nanometers in the UV–Vis and fluorescence emission spectra. Because of the introduction of metal cations within the P core (forming PEF-PZn and PEF-PCo derivatives), the polymeric sensor systems became sensitive to electron-donor species, such as amine.

The sensing response of both PEF-PZn and PEF-PCo in toluene solution depends on the chemical nature of the pollutant. Investigations with aromatic (pyridine) or non-aromatic (piperidine) pollutants demonstrated higher sensitivity to non-aromatic amines, as evidenced by more pronounced spectral modification. Furthermore, due to cobalt electronic configuration, the PEF-PCo system showed enhanced sensitivity ($LOD_{pyridine}$ = 0.16 μM; $LOD_{piperidine}$ = 0.04 μM) to both pyridine and piperidine compared to PEF-PZn ($LOD_{pyridine}$ = 22 μM; $LOD_{piperidine}$ = 0.5 μM).

The optical sensing capabilities were further validated in the solid state against gaseous pollutants, showing spectral shift and intensity enhancements of the Soret absorption band of the polymeric sensor after 1 min of exposure. The experimental data support the potential application of these systems, also as thin films, as optical sensors for amine pollutants.

CRediT authorship contribution statement

Lidia Mezzina: Writing – original draft, Visualization, Resources, Investigation, Formal analysis, Data curation. **Angelo Nicosia:** Writing – review & editing, Writing – original draft, Visualization, Validation, Resources, Project administration, Methodology, Data curation, Conceptualization. **Placido G. Mineo:** Writing – review & editing, Writing – original draft, Visualization, Validation, Supervision, Resources, Project administration, Methodology, Funding acquisition, Conceptualization.

Declaration of competing interest

The authors declare that they have no known competing financial interests or personal relationships that could have appeared to influence the work reported in this paper.

Acknowledgements

The authors thanks Simone Milazzo for his support during the earlier stages of the project.

This work has been funded by European Union (NextGeneration EU), through the MUR-PNRR project SAMOTHRACE (ECS00000022).

Appendix A. Supplementary data

Supplementary data to this article can be found online at https://doi.org/10.1016/j.dyepig.2025.112867.

Data availability

Data will be made available on request.

References

[1] Zheng H, Kong S, Yan Y, Chen N, Yao L, Liu X, et al. Compositions, sources and health risks of ambient volatile organic compounds (VOCs) at a petrochemical industrial park along the Yangtze River. Sci Total Environ 2020;703. https://doi.org/10.1016/j.scitotenv.2019.135505.
[2] Mirzaei A, Leonardi SG, Neri G. Detection of hazardous volatile organic compounds (VOCs) by metal oxide nanostructures-based gas sensors: a review. Ceram Int 2016;42(14):15119–41. https://doi.org/10.1016/j.ceramint.2016.06.145.
[3] O'Neill DH, Phillips VR. A review of the control of odour nuisance from livestock buildings: part 3, properties of the odorous substances which have been identified in livestock wastes or in the air around them. J Agric Eng Res 1992;53:23–50. https://doi.org/10.1016/0021-8634(92)80072-z.
[4] Rappert S, Müller R. Odor compounds in waste gas emissions from agricultural operations and food industries. Waste Manag 2005;25(9):887–907. https://doi.org/10.1016/j.wasman.2005.07.008.
[5] Li Z, Zhou R, Wang Y, Wang G, Chen M, Li Y, et al. Characteristics and sources of amine-containing particles in the urban atmosphere of Liaocheng, a seriously polluted city in North China during the COVID-19 outbreak. Environ Pollut 2021;289. https://doi.org/10.1016/j.envpol.2021.117887.
[6] Passant NR, Richardson SJ, Swannell RPJ, Gibson N, Woodfield MJ, van der Lugt JP, et al. Emissions of volatile organic compounds (VOCs) from the food and drink industries of the European community. Atmos Environ Part A Gen Top 1993;27(16):2555–66. https://doi.org/10.1016/0960-1686(93)90029-x.
[7] Liu Z, Li M, Wang X, Liang Y, Jiang Y, Chen J, et al. Large contributions of anthropogenic sources to amines in fine particles at a coastal area in northern China in winter. Sci Total Environ 2022;839. https://doi.org/10.1016/j.scitotenv.2022.156281.
[8] Santos MHS. Biogenic amines: their importance in foods. Int J Food Microbiol 1996;29(2–3):213–31. https://doi.org/10.1016/0168-1605(95)00032-1.
[9] Alexanderova ON. A new insight into a problem of mediating effects of humic acids on binding and biological effects of organic pollutants in natural soil. J Soils Sediments 2015;16(4):1316–22. https://doi.org/10.1007/s11368-015-1195-2.
[10] Shalaby AR. Significance of biogenic amines to food safety and human health. Food Res Int 1996;29(7):675–90. https://doi.org/10.1016/S0963-9969(96)00066-X.
[11] Bedia Erim F. Recent analytical approaches to the analysis of biogenic amines in food samples. TrAC, Trends Anal Chem 2013;52:239–47. https://doi.org/10.1016/j.trac.2013.05.018.
[12] D B, Dey D, T LV, Thodi F, Salfeena C, Panda MK, Somappa SB. Rapid visual detection of amines by pyrylium salts for food spoilage taggant. ACS Appl Bio Mater 2020;3(2):772–8. https://doi.org/10.1021/acsabm.9b00711.
[13] Mohamed MG, Basit A, Madhu M, Aravinthkumar K, Said AI, Manoj D, et al. Conjugated microporous polymer containing pyrene and dibenzo[g,p]chrysene moieties as a luminescent powerhouse for multi-target sensing and environmental safety. Microporous Mesoporous Mater 2025;391. https://doi.org/10.1016/j.micromeso.2025.113620.
[14] Nicosia A, Vento F, Satriano C, Villari V, Micali N, Cucci LM, et al. Light-triggered polymeric nanobombs for targeted cell death. ACS Appl Nano Mater 2020;3(2):1950–60. https://doi.org/10.1021/acsanm.9b02552.
[15] Han J, Liu Y, Peng D, Liu J, Wu D. Biomedical application of porphyrin-based amphiphiles and their self-assembled nanomaterials. Bioconjug Chem 2023;34(12):2155–80. https://doi.org/10.1021/acs.bioconjchem.3c00432.
[16] Imran M, Ramzan M, Qureshi AK, Khan MA, Tariq M. Emerging applications of porphyrins and metalloporphyrins in biomedicine and diagnostic magnetic resonance imaging. Biosensors 2018;8(4). https://doi.org/10.3390/bios8040095.
[17] Paolesse R, Nardis S, Monti D, Stefanelli M, Di Natale C. Porphyrinoids for chemical sensor applications. Chem Rev 2016;117(4):2517–83. https://doi.org/10.1021/acs.chemrev.6b00361.
[18] Micali N, Mineo P, Vento F, Nicosia A, Villari V. Supramolecular structures formed in water by graphene oxide and nonionic PEGylated porphyrin: interaction mechanisms and fluorescence quenching effects. J Phys Chem C 2019;123(42):25977–84. https://doi.org/10.1021/acs.jpcc.9b06800.
[19] Norvaiša K, Kielmann M, Senge MO. Porphyrins as colorimetric and photometric biosensors in modern bioanalytical systems. Chembiochem 2020;21(13):1793–807. https://doi.org/10.1002/cbic.202000067.
[20] Purrello R, Gurrieri S, Lauceri R. Porphyrin assemblies as chemical sensors. Coord Chem Rev 1999;190–192:683–706. https://doi.org/10.1016/s0010-8545(99)00106-x.
[21] Prabphal J, Vilaivan T, Praneenararat T. Fabrication of a paper-based turn-off fluorescence sensor for Cu2+Ion from a pyridinium porphyrin. ChemistrySelect 2018;3(3):894–9. https://doi.org/10.1002/slct.201702382.
[22] Wang E, Meyerhoff ME. Anion selective optical sensing with metalloporphyrin-doped polymeric films. Anal Chim Acta 1993;283(2):673–82. https://doi.org/10.1016/0003-2670(93)85281-n.

[23] Mezzina L, Nicosia A, Barone L, Vento F, Mineo PG. Water-soluble star polymer as a potential photoactivated nanotool for lysozyme degradation. Polymers 2024;16(2). https://doi.org/10.3390/polym16020301.

[24] Strianese M, Pappalardo D, Mazzeo M, Lamberti M, Pellecchia C. The contribution of metalloporphyrin complexes in molecular sensing and in sustainable polymerization processes: a new and unique perspective. Dalton Trans 2021;50 (23):7898–916. https://doi.org/10.1039/d1dt00841b.

[25] Altmann A, Eden M, Hüttmann G, Schell C, Rahmanzadeh R. Porphyrin-based sensor films for monitoring food spoilage. Food Packag Shelf Life 2023;38. https://doi.org/10.1016/j.fpsl.2023.101105.

[26] Nicosia A, Abbadessa A, Vento F, Mazzaglia A, Mineo PG. Silver nanoparticles decorated with PEGylated porphyrins as potential theranostic and sensing agents. Materials 2021;14(11). https://doi.org/10.3390/ma14112764.

[27] Lvova L, Di Natale C, Paolesse R. Porphyrin-based chemical sensors and multisensor arrays operating in the liquid phase. Sensor Actuator B Chem 2013; 179:21–31. https://doi.org/10.1016/j.snb.2012.10.014.

[28] Ruppel JV, Kamble RM, Zhang XP. Cobalt-catalyzed intramolecular C−H amination with arylsulfonyl azides. Org Lett 2007;9(23):4889–92. https://doi.org/10.1021/ol702265h.

[29] Sakuma T, Sakai H, Araki Y, Wada T, Hasobe T. Control of local structures and photophysical properties of zinc porphyrin-based supramolecular assemblies structurally organized by regioselective ligand coordination. Phys Chem Chem Phys 2016;18(7):5453–63. https://doi.org/10.1039/c5cp07110k.

[30] Zaitseva SV, Zdanovitch SA, Koifman OI. Coordination properties of zinc 5,15-di (ortho-aminophenyl)octaalkylporphyrin in reactions with mono- an dibasic nitrogen bases. Russ J Inorg Chem 2010;55(10):1574–80. https://doi.org/10.1134/s0036023610100141.

[31] Micali N, Villari V, Mineo P, Vitalini D, Scamporrino E, Crupi V, et al. Aggregation phenomena in aqueous solutions of uncharged star polymers with a porphyrin core. J Phys Chem B 2003;107(21):5095–100. https://doi.org/10.1021/jp026999p.

[32] Villari V, Micali N, Nicosia A, Mineo P. Water-soluble non-ionic PEGylated porphyrins: a versatile category of dyes for basic science and applications. Top Curr Chem 2021;379(5). https://doi.org/10.1007/s41061-021-00348-4.

[33] Ma H, Sun S, Chen X, Wu D, Zhu P, Du B, et al. Spectroscopic studies of aggregation behavior of meso-tetra(4-hydroxyphenyl)porphyrin in aqueous AOT solution. J Porphyr Phthalocyanines 2012;12(2):101–8. https://doi.org/10.1142/s1088424608000133.

[34] Cardoso WS, Francisco MSP, Landers R, Gushikem Y. Co (II) porphyrin adsorbed on SiO2/SnO2/phosphate prepared by the sol–gel method. Electrochim Acta 2005;50 (22):4378–84. https://doi.org/10.1016/j.electacta.2005.02.001.

[35] Bhaduri SN, Ghosh D, Debnath S, Biswas R, Chatterjee PB, Biswas P. Copper(II)-Incorporated porphyrin-based porous organic polymer for a nonenzymatic electrochemical glucose sensor. Inorg Chem 2023;62(10):4136–46. https://doi.org/10.1021/acs.inorgchem.2c04072.

[36] Aly KI, Sayed MM, Mohamed MG, Kuo SW, Younis O. A facile synthetic route and dual function of network luminescent porous polyester and copolyester containing porphyrin moiety for metal ions sensor and dyes adsorption. Microporous Mesoporous Mater 2020;298. https://doi.org/10.1016/j.micromeso.2020.110063.

[37] Maqueira L, Valdés AC, Iribarren A, de Melo CP. Preparation and characterization of hydrophobic porphyrin nanoaggregates dispersed in polyvinyl alcohol films. J Porphyr Phthalocyanines 2013;17(4):283–8. https://doi.org/10.1142/s1088424613500028.

[38] Vento F, Nicosia A, Mezzina L, Raciti G, Gulino A, Condorelli M, et al. Photocatalytic activity of TiO2-Containing nanocomposites versus the chemical nature of the polymeric matrices: a comparison. Advan Mater Technol 2023;8(17). https://doi.org/10.1002/admt.202300391.

[39] Wang L, Meyerhoff ME. Polymethacrylate polymers with appended aluminum(III)-tetraphenylporphyrins: synthesis, characterization and evaluation as macromolecular ionophores for electrochemical and optical fluoride sensors. Anal Chim Acta 2008;611(1):97–102. https://doi.org/10.1016/j.aca.2008.01.070.

[40] Eigner AA, Massari AM. Probing phase segregation in porphyrin-polymer blends with multidimensional ir spectroscopy. Annual international conference of the IEEE engineering in medicine and biology Society2009. 2009. p. 6307–10.

[41] Segawa H, Shimidzu T, Honda K-i. Control of π-Radical anion state of porphyrin with a polymer matrix. Polym J 1988;20(6):441–6. https://doi.org/10.1295/polymj.20.441.

[42] Mezzina L, Nicosia A, Vento F, De Guidi G, Mineo PG. Photosensitized thermoplastic nano-photocatalysts active in the visible light range for potential applications inside extraterrestrial facilities. Nanomaterials 2022;12(6). https://doi.org/10.3390/nano12060996.

[43] Duong PHH, Anjum DH, Peinemann K-V, Nunes SP. Thin porphyrin composite membranes with enhanced organic solvent transport. J Membr Sci 2018;563: 684–93. https://doi.org/10.1016/j.memsci.2018.04.038.

[44] Vitalini D, Spina E, Rapisardi R, Scamporrino E, Mineo P. Synthesis and matrix-assisted laser desorption/ionization time-of-flight characterization of bisphenol-a copolyformals containing nickel(II)/Schiff base, eicosane and 2-butene units in the main chain. Rapid Commun Mass Spectrom 2006;20(19):2961–8. https://doi.org/10.1002/rcm.2657.

[45] Mineo P, Scamporrino E, Spina E, Vitalini D. Synthesis and characterization of copolyformals containing electron-rich or electron-poor porphyrin units in the main chain and their use as sensors. Sensor Actuator B Chem 2013;188:1284–92. https://doi.org/10.1016/j.snb.2013.08.009.

[46] Nock LA, Goldwasser JM, Adolph HG. Nitro- and fluoropolyformals. III. Copolyformals from mixtures of fluoro- and nitro-α,ω-diols. J Polym Sci Polym Chem 2003;29(8):1133–49. https://doi.org/10.1002/pola.1991.080290807.

[47] Mamtmin G, Abdurahman R, Yan Y, Nizamidin P, Yimit A. A highly sensitive and selective optical waveguide sensor based on a porphyrin-coated ZnO film. Sensor Actuator Phys 2020;309. https://doi.org/10.1016/j.sna.2020.111918.

[48] Winnischofer H, de Souza Lima S, Araki K, Toma HE. Electrocatalytic activity of a new nanostructured polymeric tetraruthenated porphyrin film for nitrite detection. Anal Chim Acta 2003;480(1):97–107. https://doi.org/10.1016/s0003-2670(02)01594-5.

[49] Routledge TJ, Lidzey DG, Buckley AR. Ultrasonic spray coating as an approach for large-area polymer OLEDs: the influence of thin film processing and surface roughness on electrical performance. AIP Adv 2019;9(1). https://doi.org/10.1063/1.5082791.

[50] Vitalini D, Mineo P, Scamporrino E. Synthesis and characterization of some main chain porphyrin copolyformals, based on bisphenol A and long linear aliphatic units, having a low glass transition temperature. Macromolecules 1999;32(1):60–9. https://doi.org/10.1021/ma980834q.

[51] Scamporrino E, Mineo P, Dattilo S, Vitalini D, Spina E. Uncharged water-soluble metal-bis-porphyrins like molecular tweezers for amino acids. Macromol Rapid Commun 2007;28(15):1546–52. https://doi.org/10.1002/marc.200700234.

[52] Mineo P, Vitalini D, Scamporrino E, Bazzano S, Alicata R. Effect of delay time and grid voltage changes on the average molecular mass of polydisperse polymers and polymeric blends determined by delayed extraction matrix-assisted laser desorption/ionization time-of-flight mass spectrometry. Rapid Commun Mass Spectrom 2005;19(19):2773–9. https://doi.org/10.1002/rcm.2123.

[53] Vitalini D, Mineo P, Scamporrino E. Effect of combined changes in delayed extraction time and potential gradient on the mass resolution and ion discrimination in the analysis of polydisperse polymers and polymer blends by delayed extraction matrix-assisted laser desorption/ionization time-of-flight mass spectrometry. Rapid Commun Mass Spectrom 1999;13(24):2511–7. https://doi.org/10.1002/(sici)1097-0231(19991230)13:24<2511::Aid-rcm819>3.0.Co;2-y.

[54] Scamporrino E, Vitalini D, Mineo P. Synthesis and MALDI-TOF MS characterization of high molecular weight Poly(1,2-dihydroxybenzene phthalates) obtained by uncatalyzed bulk polymerization of O,O'-Phthalid-3-ylidenecatechol or 4-Methyl-O,O'-phthalid-3-ylidenecatechol. Macromolecules 1996;29(17):5520–8. https://doi.org/10.1021/ma960051+.

[55] Scamporrino E, Maravigna P, Vitalini D, Mineo P. A new procedure for quantitative correction of matrix-assisted laser desorption/ionization time-of-flight mass spectrometric response. Rapid Commun Mass Spectrom 1998;12(10):646–50. https://doi.org/10.1002/(sici)1097-0231(19980529)12:10<646::Aid-rcm208>3.0.Co;2-c.

[56] Mineo PG, Foti C, Vento F, Montesi M, Panseri S, Piperno A, et al. Salinomycin-loaded PLA nanoparticles: drug quantification by GPC and wave voltammetry and biological studies on osteosarcoma cancer stem cells. Anal Bioanal Chem 2020;412 (19):4681–90. https://doi.org/10.1007/s00216-020-02721-6.

[57] Menges F. Spectragryph - optical spectroscopy software, Version 1211; 2019. https://www.effemm2.de/spectragryph/.

[58] Chen J, Li H, Zhang H, Liao X, Han H, Zhang L, et al. Blocking-cyclization technique for precise synthesis of cyclic polymers with regulated topology. Nat Commun 2018;9(1). https://doi.org/10.1038/s41467-018-07754-1.

[59] Montenegro-Burke JR, Bennett JM, McLean JA, Hercules DM. Novel behavior of the chromatographic separation of linear and cyclic polymers. Anal Bioanal Chem 2015;408(3):677–81. https://doi.org/10.1007/s00216-015-9198-9.

[60] Deffieux A, Schappacher M. Synthesis and properties of macrocyclic polymers. In: Polymer Science: A Comprehensive Reference; 2012. p. 5–28.

[61] Si J, Hao N, Zhang M, Cheng S, Liu A, Li L, et al. Universal synthetic strategy for the construction of topological polystyrenesulfonates: the importance of linkage stability during sulfonation. ACS Macro Lett 2019;8(6):730–6. https://doi.org/10.1021/acsmacrolett.9b00260.

[62] Montaudo G, Puglisi C, Scamporrino E, Vitalini D. Thermal degradation of aromatic-aliphatic polyethers. 1. Direct pyrolysis-mass spectrometry. Macromolecules 1986;19(3):870–82. https://doi.org/10.1021/ma00157a067.

[63] Corres MA, Zubitur M, Cortazar M, Múgica A. Thermal and thermo-oxidative degradation of poly(hydroxy ether of bisphenol-A) studied by TGA/FTIR and TGA/MS. J Anal Appl Pyrolysis 2011;92(2):407–16. https://doi.org/10.1016/j.jaap.2011.08.002.

[64] Nicosia A, Vento F, Marletta G, Messina G, Satriano C, Villari V, et al. Porphyrin-based supramolecular flags in the thermal gradients' wind: what breaks the symmetry, how and why. Nanomaterials 2021;11(7). https://doi.org/10.3390/nano11071673.

[65] Spellane PJ, Gouterman M, Antipas A, Kim S, Liu YC. Porphyrins. 40. Electronic spectra and four-orbital energies of free-base, zinc, copper, and palladium tetrakis (perfluorophenyl)porphyrins. Inorg Chem 2002;19(2):386–91. https://doi.org/10.1021/ic50204a021.

[66] Makarska M, Radzki S, Legendziewicz J. Spectroscopic characterization of the water-soluble cationic porphyrins and their complexes with Cu(II) in various solvents. J Alloys Compd 2002;341(1–2):233–8. https://doi.org/10.1016/s0925-8388(02)00099-3.

[67] Liu X, Tripathy U, Bhosale SV, Langford SJ, Steer RP. Photophysics of soret-excited tetrapyrroles in solution. II. Effects of perdeuteration, substituent nature and position, and macrocycle structure and conformation in Zinc(II) porphyrins. J Phys Chem 2008;112(38):8986–98. https://doi.org/10.1021/jp804792x.

[68] Farajtabar A, Jaberi F, Gharib F. Preferential solvation and solvation shell composition of free base and protonated 5, 10, 15, 20-tetrakis(4-sulfonatophenyl) porphyrin in aqueous organic mixed solvents. Spectrochim Acta Part A: Mol Biomol Spectrosc 2011;83(1):213–20. https://doi.org/10.1016/j.saa.2011.08.020.

[69] Bhyrappa P, Sankar M. Effect of solvent on the electronic absorption spectral properties of some mixed β-octasubstituted Zn(II)-tetraphenylporphyrins.

Spectrochim Acta Part A: Mol Biomol Spectrosc 2018;189:80–5. https://doi.org/10.1016/j.saa.2017.07.059.
[70] El-Refaey A, Shaban SY, El-Kemary M, El-Khouly ME. Spectroscopic and thermodynamic studies of light harvesting perylenediimide derivative - zinc porphyrin complex in aqueous media. Spectrochim Acta Part A: Mol Biomol Spectrosc 2017;186:132–9. https://doi.org/10.1016/j.saa.2017.06.016.
[71] Jeong J, Satish Kumar R, Naveen M, Son Y-A. Synthesis, thermochromic, solvatochromic and axial ligation studies of Zn-porphyrin complex. Inorg Chim Acta 2018;469:453–60. https://doi.org/10.1016/j.ica.2017.10.004.
[72] Polfer NC, Oomens J, Moore DT, von Helden G, Meijer G, Dunbar RC. Infrared spectroscopy of phenylalanine Ag(I) and Zn(II) complexes in the gas phase. J Am Chem Soc 2005;128(2):517–25. https://doi.org/10.1021/ja0549291.
[73] Shmilovits M, Vinodu M, Goldberg I. Coordination polymers of Tetra(4-carboxyphenyl)porphyrins sustained by tetrahedral zinc ion linkers. Cryst Growth Des 2004;4(3):633–8. https://doi.org/10.1021/cg0342009.
[74] Berezin DB, Zharnikova NV, Andrianov VG, Shatunov PA, Semeikin AS. Coordination of N-Substituted porphyrins with simple and chelate zinc salts in DMSO. Russ J Coord Chem 2002;28(5):325–32. https://doi.org/10.1023/a:1015565132623.
[75] Rivera JM, Rivera M. Tetraphenyl porphyrin films as selective detectors for amino acid molecules. J Porphyr Phthalocyanines 2020;24(10):1215–23. https://doi.org/10.1142/s1088424620500340.
[76] Guseva LZ, Pukhovskaya SG, Golubchikov OA. Coordination of pyridine and piperidine by cobalt complexes of water-soluble porphyrin and phthalocyanines. Russ J Inorg Chem 2010;55(4):552–5. https://doi.org/10.1134/s0036023610040108.
[77] Walker FA. Steric and electronic effects in the coordination of amines to a cobalt(II) porphyrin. J Am Chem Soc 2002;95(4):1150–3. https://doi.org/10.1021/ja00785a025.
[78] Walker FA. Reactions of monomeric cobalt-oxygen complexes. I. Thermodynamics of reaction of molecular oxygen with five- and six-coordinate amine complexes of a cobalt porphyrin. J Am Chem Soc 2002;95(4):1154–9. https://doi.org/10.1021/ja00785a026.
[79] He L, He J, Chen E-X, Lin Q. Boosting photothermal conversion through array aggregation of metalloporphyrins in bismuth-based coordination frameworks. Chem Sci 2024;15(42):17498–505. https://doi.org/10.1039/d4sc04063e.
[80] Mizutani T, Wada K, Kitagawa S. Molecular recognition of amines and amino esters by zinc porphyrin receptors: binding mechanisms and solvent effects. J Org Chem 2000;65(19):6097–106. https://doi.org/10.1021/jo000557x.
[81] Bhyrappa P, Krishnan V, Nethaji M. Solvation and axial ligation properties of (2,3,7,8,12,13,17,18-octabromo-5,10,15,20-tetraphenylporphyrinato)zinc(II). J Chem Soc, Dalton Trans 1993;(12). https://doi.org/10.1039/dt9930001901.